Approach to surface structure determination with the scanning tunneling microscope: Multiple-gap imaging and electron-scattering quantum-chemistry theory

J. C. Dunphy
Department of Physics, University of California, Berkeley, Berkeley, California 94720

P. Sautet
Laboratoire de Chimie Théorique, ENS Lyon, 69364 Lyon, France
and Institut de Recherche sur la Catalyse, 69626 Villeurbanne, France

D. F. Ogletree and M. Salmeron*
Center for Advanced Materials, Material Science Division, Lawrence Berkeley Laboratory, Berkeley, California 94720
(Received 27 April 1995; revised manuscript received 26 June 1995)

We have successfully developed and tested a method of quantitative surface structure determination using scanning tunneling microscopy (STM). Image simulations of the $c(2\times2)$ S on Mo(100) chemisorption system were calculated as a function of surface and tip structure using electron-scattering quantum-chemistry STM theory. STM images with a wide range of tunneling gap resistance values were acquired in a "multiple-gap" mode which preserves information on the z separation and lateral registry between the images under different tunneling conditions. The best fit of a numerical comparison of the image simulations with experimental data simultaneously determined two structural parameters of the surface. The STM results differ from those of dynamical LEED by approximately 0.1 Å, which we estimate to be the level of accuracy obtainable with the present implementation of the method.

I. INTRODUCTION

The understanding of the electronic, physical, and chemical properties of surfaces requires an accurate knowledge of their atomic level structure. A number of methods are now routinely used to determine the adsorption sites and bond lengths of adsorbates on metal surfaces. These include low-energy electron diffraction (LEED),[1] ion scattering,[2] x-ray photoelectron diffraction (XPD),[3] and surface-extended x-ray-absorption fine structure (SEXAFS).[4] When coupled with appropriate theoretical modeling, these methods provide information on either the average surface structure or the structure of well-ordered portions of the surface. However, it is generally believed that many of the properties of surfaces are a consequence of defect sites which may be present in low concentration and randomly distributed. As a real-space technique, scanning tunneling microscopy (STM) has the ability to focus on a specific region of the surface, such as a defect site, isolated adsorbate atom, or antiphase boundary. The ability to study nonperiodic surface features gives this technique the potential to provide structural information unavailable by other methods. However, to our knowledge no general technique for deriving the complete surface structure from STM images has been developed.

Some information on surface structure can be immediately determined by inspection of STM images. It is simple to measure the distance between equivalent points on the surface, both laterally and in height. These measurements provide the periodicity of the surface and the separation of atomic layers (step height). Additionally, the binding site of adsorbate atoms (top, hollow, or bridge) may often be determined from an analysis of the symmetry of the images, especially at defect sites and antiphase boundaries.[5] In contrast, STM does not directly yield information about the relative positions of inequivalent atoms, such as the bond length between adsorbate and substrate atoms or the distance between adsorbate atoms bound at different surface sites. This is because STM does not produce a simple image of a hard-sphere model of the surface, but a map of tip-surface conductance which is a combination of physical and electronic structure. Other factors besides the surface structure may influence the image contrast, including the tunneling conditions (bias voltage and tunneling current) and the morphology of the tip termination.[5–9] A theoretical approach is needed to separate this electronic structure influence on the image from the physical structure of the surface.

Considerable effort has been focused on developing an accurate theoretical description of electron tunneling with which STM images can be calculated.[10–20] Most early models of tunneling described the tip and surface with free-electron models which do not have atomic structure.[11–14] Other approaches use more accurate descriptions of the surface and tip physical and electronic structure, but most use Bardeen's approximation,[21] a perturbation approach, to calculate the tunneling current. Using this approximation, Tersoff and Hamann showed that STM images may be approximated by the surface electron density at the Fermi level at the center of a tip modeled by a single s wave function.[16] Lang improved the description of the tip, modeling the tip and surface as atoms embedded in jellium and calculating the electronic states with the local-density approximation (LDA).[17,18]

Tsudaka *et al.* have developed a model using a linear combination of atomic orbitals (LCAO) description of the wave function of the surface and a tip cluster coupled to a specialized model of the vacuum tail. Other theories avoid Bardeen's approximation, taking the tip-surface interactions into account, which is especially important for accurate modeling of tunneling with a small tip-surface separation. These include the theories of Doyen, Drakova, and Scheffler[15] and Sautet and Joachim,[19,20] which accurately include the influence of the tip-surface electronic interaction by modeling the surface and tip with atomic orbitals and treating the electron tunneling between them with a scattering theory.

Despite the development of these theoretical methods, STM theory has only rarely been applied to deduce surface structure from STM images. Feenstra *et al.* used the Tersoff and Hamann[16] approach to determine the buckling angle of bonds on the GaAs surface.[22] STM images acquired with positive and negative bias voltages were compared to calculations of the surface density of states as a function of the bond angle. In our previous work, a partial structural determination was made for the $p(2\times2)$S on the Re(0001) chemisorption system.[23,24] The experimental images of this system were consistent with calculated images only for a small range of trial surface structures. From the comparison of the experimental and calculated images, the binding site of the adsorbed sulfur atom was determined to be the threefold hollow site. The height of the sulfur over the surface was limited to within the small range from 1.60 to 1.75 Å above the first Re layer. The results agree closely with those of a dynamical LEED structure determination.[25]

An important result of this theoretical work has been the improved understanding of the mechanisms of contrast in STM images.[23] The contrast was found to be modified by electronic interferences among several tunneling paths between the surface and the tip. In general, atomic orbitals of more than one surface atom may overlap significantly with the atomic orbitals of the tip termination atom. The tunneling amplitudes of electrons for these paths are complex quantities which may interfere, significantly enhancing or reducing the tunneling current compared to the sum of the individual paths. This electronic interference of states with approximately the Fermi wavelength ($\sim$1 Å) makes the STM contrast sensitive to the geometry of the tunneling gap region with a resolution of fraction of this wavelength, of order 0.1 Å. In principle, this fact allows quantitative information on the structure of the surface to be obtained from the contrast in STM images.

Here a comparison of experimental STM images with those calculated by an electron-scattering theory is used quantitatively to determine the structure of the $c(2\times2)$S on Mo(100) system. We begin with a model structure assuming that S is bound at the fourfold hollow site as it has been found to bind at the highest coordination site on nearly all metal surfaces studied to date.[26] Two parameters of the structure are optimized by fitting the STM data: the height of the bound sulfur and the buckling of the second Mo layer. Unlike previous work on the S on Re system, a quantitative approach is used for the comparison of theoretical images with calculated ones. In addition, the images are obtained at more than one tunneling condition, enlarging the experimental data set.

II. APPROACH

Our approach to STM structure determination is analogous to that of dynamical LEED. As with STM image data, there is no way to directly invert LEED $I(V)$ curves to real-space surface structure. Instead, a multiple-scattering theory is used to calculate $I(V)$ curves for each of a large set of trial structures. Each of these curves is numerically compared to the experimental one by calculating an R factor representing the quality of the fit. The trial structure which has the best R factor is presumed to be the correct structure.

In the STM approach, images are calculated as a function of surface structure, tip structure, and tunneling conditions for a set of trial structures. The surface structure is determined from the best fit between these calculations and the experimental STM data. As a single unit cell of a STM image has few distinct features, we enlarge the data set by obtaining simultaneously a set of images with different tunneling conditions. The complete set of images is fit to an equivalent set of calculated images.

Two tunneling parameters may be controlled by the experimenter: the bias voltage and the tunneling current (or gap resistance). Changing the bias voltage modifies the energy overlap of the states of the surface and tip. In systems, such as semiconductors, in which the density of states or their wave functions vary rapidly with energy, changes in the bias voltage will have a pronounced effect on the image contrast. However, metals have a relatively flat density of states near the Fermi level, and hence changing the bias voltage has little effect on the image. Experimentally, this was verified for the S on Mo system. Inverting the bias voltage from $+0.2$ to -0.2 V produced almost no measurable change in the image contrast.

On the other hand, changing the gap resistance (through variation of the tunneling current), does have an effect on the image contrast of adsorbates on metals. Changes in the gap resistance result in a shift in tip-surface separation. The separation varies approximately linearly with the logarithm of the gap resistance. Changing the distance between the tip and surface modifies the interference between different tunneling paths, resulting in image contrast variations. Different surface structures will have different degrees and forms of interference change with tip height. Therefore, acquiring data at multiple tunneling gaps provides additional information on surface structure beyond what an image at a single tunneling gap can provide.

In order to maximize the amount of experimental data, images were acquired over a wide range of tunneling gap resistance values at a low fixed bias voltage. The gap resistance was modified by changing the tunneling current setpoint of the feedback loop controlling the tip z position. A special parallel image acquisition mode was implemented which preserves information on the relative

z separation and registry of images acquired at different tunneling gap resistance values.

An additional factor which may vary in the STM experiment is the structure of the STM tip termination. Unfortunately this structure is largely beyond the control and knowledge of the experimenter. Therefore, a number of likely model tip termination structures must be used in the theoretical image simulation. The fit between the experiment and theory must simultaneously determine the surface structure and at least part of the structure of the tip.

III. ESQC STM THEORY

The simulated STM images were calculated using the electron-scattering quantum-chemistry (ESQC) theory.[19,20] This theory has been employed to calculate STM images on a wide range on systems with a high degree of success. As previously described, this theory was successfully applied to the $p(2\times2)$S on Re(0001) system. The theory has also correctly predicted the shape of benzene[27] and CO[28] molecules adsorbed at different sites on the Pt(111) surface. While it has proven to be highly accurate, ESQC theory is capable of simulating STM images of a simple surface structure in less than 1 h of computer time on a standard workstation. This computational efficiency is required for application to structural determination, where it is necessary to calculate the STM images of a large number of possible structures. In addition, unlike in some of the approaches to calculating STM images outlined above, ESQC accurately models the surface and the tip with an atom by atom description of the bulk, surface, and tip geometries.

In ESQC theory the tunneling of electrons between the surface and tip is described as a scattering process. Electrons traveling through the bulk substrate and tip are scattered at the tunneling junction, where the periodic layer symmetry of the bulk is broken. This junction consists of the top few surface layers, the adsorbate layer, the tunneling gap, and the tip apex. Electrons in each bulk eigenstate of the surface and tip will be mostly reflected at the junction, with a very small fraction transmitted across the gap. The reflection and transmission probabilities are expressed by a scattering matrix S that describes how the gap couples the bulk electronic wave functions on each side. This matrix is clearly dependent on the junction structure, including the tip position, the tip termination morphology, and the surface structure. The gap resistance, as a function of the structure in the tip-adsorbate-surface region, is calculated from the scattering matrix in the zero-bias voltage approximation with the Landauer[29] formula. A simulated STM image is produced by plotting the reciprocal of the gap resistance as a function of lateral tip displacement.

The calculation of the scattering matrix requires that the surface, adsorbate, and tip all be considered simultaneously. The complete model system is infinite in the z direction perpendicular to the surface and has periodic boundaries in the surface (xy) plane. Each component of the system is described atom by atom. The bulk tip and sample in the present experiments are semi-infinite structures described by two layers of Mo atoms with periodic boundary conditions in the z direction. Within the surface plane the Mo bulk is described as a 4×4 atom cell with periodic boundary conditions. The surface-adsorbate-tip region consists of two layers of Mo, the adsorbate layer, and the tip apex. This region is placed between the semi-infinite bulk tip and sample sections. While the tip is formally repeated, the size of the repeated cell is large enough (4×4) so that the interactions between adjacent tips are insignificant.

Each atom in the system is associated with an orbital basis set. In the bulk, only one $5s$ orbital is used to describe the atom, while a full *spd* basis set is used in the surface and tip regions where the scattering takes place. The exponents of the Slater-type orbitals (STO's) of this basis set are taken from *ab initio* atomic calculations.[30] A tight-binding approach based on the extended Hückel theory is then used. The overlap matrix elements between these STO's are calculated with no limitation to nearest-neighbor interaction. The Hamiltonian matrix elements are approximated[31] from the overlap and from the diagonal Hamiltonian matrix elements (these atomic-orbital energies are parameters of the calculation and are taken from the literature). This approach allows a simple and fast determination of the matrix elements, and correctly takes into account the atomic-orbital overlaps and their dependence upon atomic distances. Besides the approximation in the determination of the Hamiltonian, the major limitation of this approach is its non-self-consistent character which tends to overestimate the electronic transfers. This approximation is, however, not very important for the relatively weak tip-surface interactions, and is usually corrected by using effective atomic-orbital energies in order to simulate self-consistent field effects.

By such a projection on the atomic basis, the Schrödinger equation is transformed into an infinite matrix, general eigenvalue equation. Propagators, which are transfer operators of the wave function in the z direction, are built for both the periodic bulk regions and for the entire STM gap junction. The scattering matrix is derived from these propagators. This theoretical approach completely takes into account the electronic coherence in the complete tip-surface system including multiple scattering and interference between tunneling paths.

IV. THEORY RESULTS

The model of the $c(2\times2)$S on Mo(100) surface, which is input into the theory, is shown in Fig. 1. The $c(2\times2)$ structure has the lowest S coverage of the three ordered structures formed by S on the Mo(100) surface. The models considered all have the S adsorbate atoms placed at the fourfold hollow site, consistent with a dynamical LEED structure determination of this surface.[32] The Mo surface interlayer spacing is taken from the LEED structural determination. The value of this spacing is quite close to the bulk value of 1.575 Å, so that using the bulk value would not have a significant effect on the results. Two parameters in the model are left free: the height of the sulfur adsorbate and the buckling of the

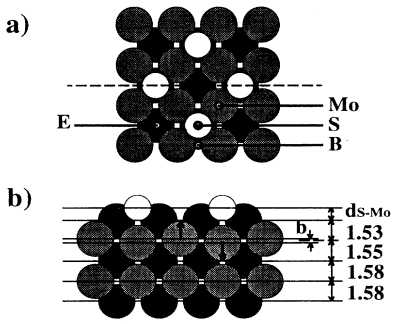

FIG. 1. A model of the $c(2\times2)$S-Mo(100) surface. (a) Top view. Every other fourfold hollow site contains a S adsorbate atom, shown in white. There are four high-symmetry sites on the surface: the location of the adsorbed sulfur atom (S), the bridge site (B), the empty hollow site (E), and over a Mo substrate atom (Mo). (b) Cross section. There are several numerical parameters which describe the surface structure. Two of these are determined by the analysis of the STM image data: the height of the sulfur atom over the surface ($d_{S\text{-}Mo}$) and the second-layer Mo buckling (b). Here the buckling (b) sign is defined as positive when the Mo atom under the sulfur adsorbate moves up toward it. (A negative buckling is indicated in the figure.) The other parameters, which specify the interlayer spacing of the Mo, are set to the values determined by a dynamical LEED study. These values are very close to the bulk layer spacing.

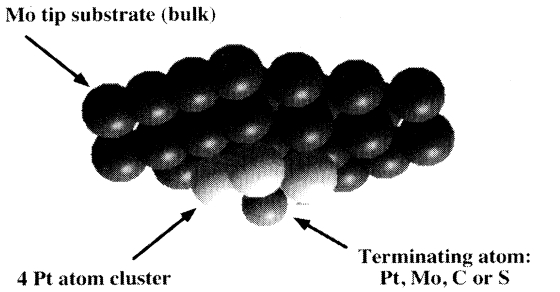

FIG. 2. Model tips used in the theory. The tip model contains three parts: the bulk, a cluster, and a termination atom. Throughout the tip all nearest-neighbor atomic separations are set to the sum of the covalent radii of the two neighbors. The bulk tip consists of Mo (the sample material) for simplicity. A four-atom Pt cluster is attached to the bulk to model the Pt alloy tip used in the experiment. A single atom is attached to this cluster. This tip termination atom is chosen from a set of likely experimental tip termination structures: Pt for a clean tip and S, C, or Mo for a contaminated tip.

second Mo layer. As half of the atoms in the second Mo layer are nearest neighbors with the sulfur adsorbate atoms while the other half are not, buckling of the second layer is expected. These two free parameters were independently varied over a likely range of values. The sulfur height over the surface was set to one of five values from 0.8 to 1.2 Å, while the second-layer buckling was picked from five values between -0.4 and $+0.4$ Å. Hence a total of 25 trial surface structures were considered.

Besides the structure of the surface, the tip structure must be input into the theory calculation. The tip is modeled as a cluster of atoms of a given composition and structure. Due to the exponential decay of the tunneling current with the distance to the surface, only the last few atoms at the tip apex contribute significantly to the tunneling current and thus to the image contrast. Therefore, the complete set of possible tips may be modeled by a smaller set of tip termination structures. The number of trial tips can be further reduced by considering only symmetrical tips terminating in one atom. Theoretical work has shown that slightly asymmetric or tilted tips produce nearly the same image contrast as completely symmetric ones.[6] Experimental data with low corrugation or which do not have the complete symmetry of the surface, known from LEED, must be a result of a more complex tip termination or multiple termination tip and can be excluded, making it unnecessary to model these complex tips in the theory.

The model tip we used is shown in Fig. 2. Since the bulk tip composition has no effect on image contrast, it can be modeled as any conductor. For simplicity, the theory uses the same material and crystal structure as the bulk sample, bcc molybdenum.

Attached to the end of the bulk tip, near the tunneling gap, is a cluster of Pt which is the predominant atomic species in the experimental tip (Pt/40% Rh alloy wire). A single atom is attached to the end of this cluster. The atomic identity is chosen from several likely candidates: Pt from the bulk tip and S, Mo, or C to model contaminated tips. The separation between neighboring atoms in the tip is set to the sum of the covalent radii of the neighbors. Test calculations have confirmed that small changes in this separation, even at the tip termination, produce very little change in the simulated image contrast.[24]

The complete set of image calculations were done on 25 surface structures and four tip structures for a total of 100 model systems. Each individual calculation determined the tunneling gap conductivity at four high-symmetry points of the surface overlayer unit cell over an approximately 4–6 Å range of tip-surface separations at 0.5 Å increments. The four high-symmetry points chosen, shown in Fig. 1(a), are at the sulfur adsorbate (denoted S), the empty fourfold hollow site (E), over a Mo atom (Mo), and at a bridge site (B). Every point on a 1.57-Å($\frac{1}{2}\times\frac{1}{2}$) mesh covering the surface is symmetrically equivalent to one of these points. This distance is approximately the lateral resolution of STM under optimum tunneling conditions. Hence these four points are sufficient to fully describe the shape of the surface observed by STM at a fixed tunneling gap. The complete set of data for a given tip and surface structure is a three-dimensional spatial map of the tunneling current with a resolution of 0.5 Å in z, and 1.57 Å in x and y.

Topographic images, over a four-order-of-magnitude range of tunneling gap resistance, may be easily interpolated from this map. However, for comparison with experimental data, a complete set of images is not necessary. Instead, the tip height for a set of experimental gap

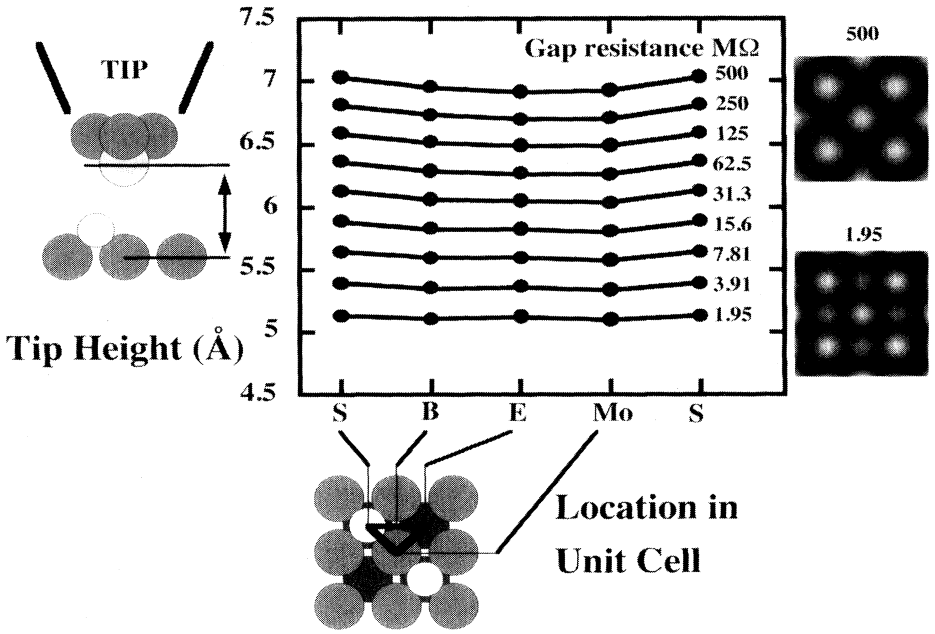

FIG. 3. Theoretical image shape plot for a single surface and tip structure. Each curve in this graph represents the distance from the tip to the surface at a specific tunneling gap resistance at the four high-symmetry sites on the surface, shown in the model below the graph. The distance between the tip and surface is defined as the distance between the center of the atom terminating the tip and the center of the first layer of Mo atoms on the surface. The tunneling gaps range from 2 to 500 MΩ by factors of 2. To the right of the plot are simulated images corresponding to the highest and lowest values of the tunneling gap. The contrast and corrugation of STM images varies markedly as a function of tunneling gap resistance.

resistance values was interpolated at each of the high-symmetry sites. The result for a single surface model and tip structure (one of the hundred) is shown in Fig. 3. The y axis of this graph is the tip height, specifically the distance between the center of the tip termination atom and the top Mo layer. On the x axis are the four high-symmetry points on the surface (one is repeated). Each curve represents the tip height over the surface as it follows the triangular path shown below the graph over the four high-symmetry points and back to its starting position while maintaining a constant tunneling gap resistance, labeled to the right of the curve. Concave-up curves represent images with a maximum at the location of the sulfur adsorbate, while concave-down curves are at a minimum at this location. In the example shown, the image contrast changes significantly with the gap resistance, as shown by the simulated images at the highest and lowest gaps.

Figure 4 displays how the contrast indicated by these curves is affected by the surface structure. The results for all of the 25 surface structures calculated for a Pt-terminated tip are displayed simultaneously. Each set of curves is similar to the plot of Fig. 3. The outer y axis represents the sulfur adsorbate height over the Mo surface, while the x axis represents the second-layer Mo buckling. As the surface structure is changed along either axis, clear changes appear in both the image shape at

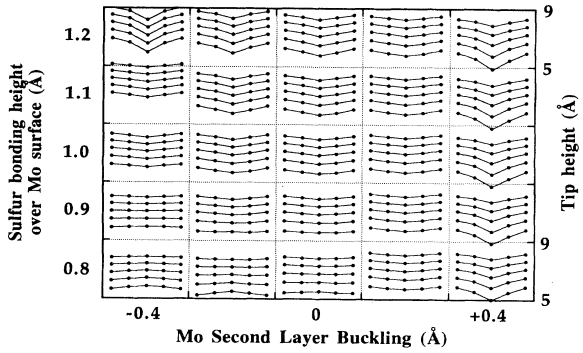

FIG. 4. Theoretical image shape plots as a function of surface structure with a Pt-atom-terminated tip. Each set of curves in this graph is equivalent to the graph in Fig. 3 for a specific structure of the surface. They indicate the tip height (labeled for several of the groups on the right y axis) at the four high-symmetry points on the surface at five values of the tunneling gap resistance. The outer x and y axes represent the two free parameters of the surface structure, the S adsorbate height, and the buckling of the second Mo layer. The changes in the shape of the groups of curves and the spacing between them indicates that the STM images are sensitive to changes in the structure of the surface. The surface structure is determined by ascertaining which set of these, compared with similar ones for other tip termination structures, best fits the experimental data.

different gap resistance values and in the decay of the tunneling current with gap distance. These curves can easily be numerically compared to analogous ones derived from our experimental STM data.

V. EXPERIMENT

The Mo sample preparation and STM imaging were performed inside a standard surface science ultrahigh-vacuum (UHV) chamber with a base pressure of 2×10^{-10} Torr. Besides the STM, the chamber was equipped with Auger electron spectroscopy (AES), LEED, and Ar^+ sputtering. The single crystal Mo(100) sample could be separately heated with an electron-beam heater, and cooled by placing the sample holder in contact with a copper block cooled by liquid nitrogen. All STM imaging took place at room temperature. The design of the STM is described elsewhere.[33] Mechanically cut Pt/Rh (60%/40%) tips were used. The tips were cleaned by applying electrical pulses of several volts between a sacrificial area of the sample and the tip when in tunneling range.

The single-crystal sample was approximately 1 cm in diameter and less than 1 mm thick. It was oriented to within less than 1° of the [100] direction, and polished using standard metallographic techniques. Carbon and other impurities were removed by sputtering while heating to approximately 600 K. The carbon remaining after this treatment was removed by repeated heating in oxygen (5×10^{-7} Torr at 1600 K). The remaining oxygen was removed by heating the crystal in UHV above 1900 K. In order to prevent contamination, sulfur was deposited on the clean surface by the decomposition of H_2S gas immediately after the removal of the oxygen. The sample was heated to approximately 800 K and exposed to 10 L of H_2S. After this treatment, the S coverage on the surface slightly exceeded the 0.5 ML required for the $c(2\times2)$ structure, as indicated by AES and LEED. The LEED pattern had a $c(2\times2)$ symmetry, with streaks in the $\langle 011\rangle$ directions from each of the overlayer half-order spots, indicating frequent antiphase boundaries in the overlayer.[1] The crystal was annealed in short cycles to desorb S and reorder the surface until a sharp $c(2\times2)$ LEED pattern was observed. After this preparation procedure the AES spectrum showed no trace of carbon or oxygen contamination.

As shown in the example of Fig. 5, STM images of the sample showed an array of maxima spaced by $\sqrt{2}$ of the Mo(100) surface lattice. Each maximum is therefore attributed to one unit cell of the $c(2\times2)$S overlayer, consisting of one S atom and two top-layer Mo atoms. As has been reported elsewhere,[34] S adsorption on Mo(100) was found to promote the clustering of single-atomic height steps, increasing the size of atomically flat terraces. Occasional point defects and antiphase boundaries were observed on these terraces. Point defects always appeared in the image where a current or topographic maximum would otherwise be found, indicating that the sulfur atoms are located at current maxima in the STM images, consistent with observations of sulfur on other metal surfaces.[35–37] Changes in the contrast of the image sometimes occurred during scanning, and are attributed to movement of atoms at the tip termination. The z (perpendicular to the surface) calibration of the piezoelectric element was determined by measurements of the height of single atomic steps. The calibration was calculated from the offset in z control voltage between planes fit to the terraces above and below a step. This calibration was reproducible within a single experiment to within 2%. After stable tunneling conditions were obtained with low thermal drift, images containing 30–40 S atoms total were acquired with a tunneling gap bias voltage in the range ±50 to ±150 mV.

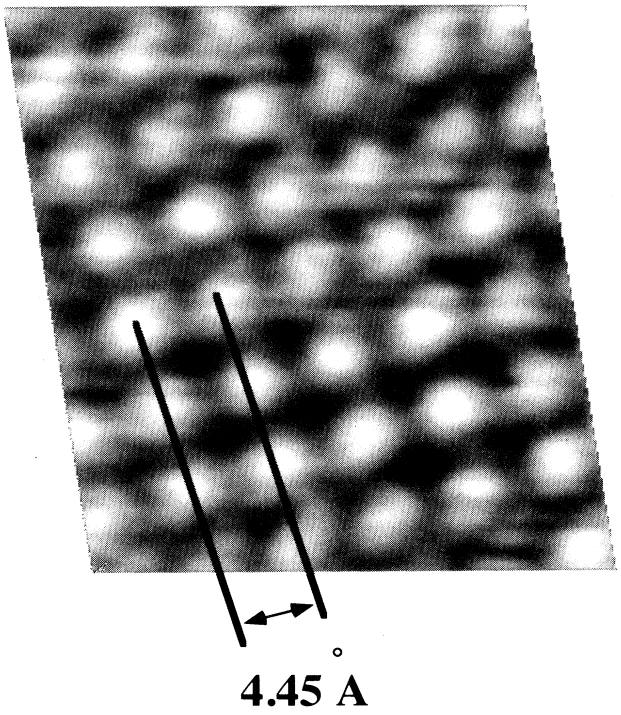

FIG. 5. A topographic STM image of $c(2\times2)$-ordered S on Mo(100). The maxima in the image are separated by 4.45 Å or $\sqrt{2}$Mo(100) lattice constants. This distance corresponds to the separation of the sulfur adsorbates. Therefore, each maximum is associated with one S and two Mo surface atoms. Defect sites in the lattice always appear as a missing maximum, indicating that the maxima correspond to the location of adsorbed S atoms.

VI. MULTIPLE-GAP IMAGING

A special mode of image acquisition, multiple-gap imaging, was used to acquire STM data over a wide range of tunneling gap resistance values. While in principle this could be accomplished by sequentially obtaining a series of images at different tunneling currents, it is not clear whether such images are generated with the same tunneling tip and are of precisely the same area of the surface. The tip termination may change between images by the diffusion of the atom at the tip end or the movement of atom between the tip and the surface. Thermal drifting of the sample relative to the tip makes an accurate deter-

mination of the relative registry and gap distance between images very difficult. These problems may be overcome by taking nearly simultaneous images at multiple tunneling gaps using a multiplexing technique.

A schematic model of this technique is shown in Fig. 6. In the multiple-gap imaging mode the tip is scanned over the surface while maintaining a constant tunneling current within each line by means of a feedback loop as in standard STM imaging. The setpoint of the feedback loop is cycled over a range of exponentially distributed current values, changing at the end of each scan line. In other words, line numbers 0, 8, 16, etc. are acquired with a tunneling current of 0.1 nA, while lines 1, 9, 17, etc. are acquired at 0.2 nA, and lines 2, 10, 18, etc. are acquired at 0.4 nA. Due to the exponential response of the tunneling gap, the gain of the feedback integrator must be changed inversely with the current setpoint in order to maintain a constant feedback loop response. Once an entire image of scan lines has been acquired, the individual lines of data were sorted by their gap resistance (or tunneling current setpoint) into separate images. As all data were acquired at the same time, any thermal drift in the lateral or z directions is the same for all the images, and a uniform correction may be applied. Therefore, the relative registry and the z displacement between the images are known. Since the images are acquired almost simultaneously (the time difference corresponds to only the time to acquire one scan line), it is certain that the tip termination which produced them is the same. Any change in the tip termination structure will appear as a contrast change at the same point in all the images. In this case the complete set of data was discarded.

VII. EXPERIMENTAL DATA

Hundreds of experimental multiple-gap images were acquired at eight tunneling gaps exponentially spaced from 2.5 to 500 MΩ. This range of 200 represents the maximum dynamic range available with our current preamplifier at which data can be acquired at low noise levels and without saturating the amplifier. The minimum gap resistance value of 2.5 MΩ was chosen as the minimum value at which it is certain that the presence of the tip will not perturb the surface, based on other experimental evidence.[38]

Much of the experimental data were discarded for one of several reasons. Any data showing defects either in the overlayer or due to atomic steps were excluded in order to avoid the complication of possible changes in surface structure in the regions surrounding these defects. Images in which the contrast was extremely low or in which the tip showed signs of instability were also discarded. The decay of the tunneling current with the gap distance was extracted from each of the remaining image sets simply by calculating the average tip height for each of the eight gap resistance values. In many cases the decay rate was found to be far less than the one order of magnitude per Å expected from the theory, and consistent with most other experiments. An example of this result is shown in Fig. 7. Additionally, these data deviated from the expected exponential behavior at small tunneling gap resistance values. Such anomalous data are attributed to tips contaminated with a nonconductive material at the contact point with the surface. During ac-

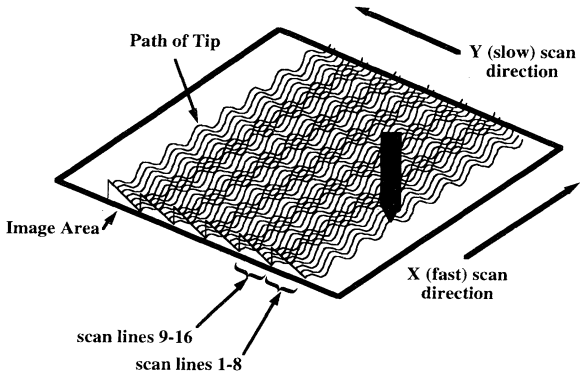

FIG. 6. A representation of the multiple-gap imaging technique. In this imaging mode the tunneling current is cycled between a small number of exponentially spaced values, changing between these values at the end of each scan line. This change in current setpoint causes the feedback loop to change the physical distance of the tunneling gap. After an entire image is acquired, the data are sorted into separate images, each corresponding to one tunneling gap resistance. This method of data acquisition has the advantage of preserving the relative position of images taken at different tunneling gap resistance values. In addition, it prevents discrepancies in the data produced by tip changes occurring between sequential images.

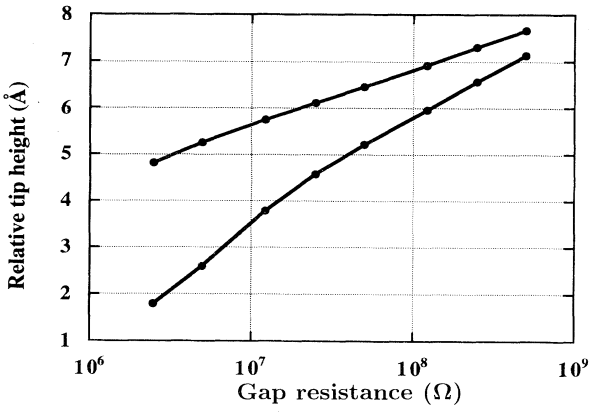

FIG. 7. The decay of the tunneling current with tip-surface spacing: normal (upper curve) and anomalous data (lower curve). Theoretical results, even from simple models, indicate that the electron wave function and hence tunneling current should decay exponentially away from the surface at a rate of approximately one order of magnitude per Å. The experimental data in the top curve are consistent with these results. Often, however, we found experimental $I(z)$ curves, showing anomalously slow decay rates and a nonexponential shape at low tunneling gaps, like the example shown in the lower curve. As explained in the text, these curves are attributed to tips contaminated with nonconducting material.

quisition of these images, the tip physically pressed against the surface, decreasing its ability to move in response to a voltage change to the piezoelectric element, especially at high current setpoints.[39] This produced a slow decay of tunneling current with changes in the apparent z position (applied control voltage). Surprisingly, these images were among those which qualitatively looked best, perhaps due to the stabilizing effect a mechanical contact has on the tunneling gap. As the theory assumes a conductive tip and does not include mechanical interactions between the tip and surface, data showing these features were excluded from comparison with the theory results.

The remaining experimental image data were processed into the same form as the theory data shown in Fig. 3. The raw data consist of multiple images with eight gap resistance values, each approximately 20×20-Å^2 size and containing around 30 unit cells of the overlayer. In order to correct for the surface slope and piezoelectric element hysteresis, a single parabolic fit is subtracted from all eight of the images, taking into account the one scan line displacement between sequential images. The maxima in the images are connected with the vertices of a $c(2\times2)$ square lattice. A second-order two-dimensional transform mapping the data space to real space was determined from a least-squares fit between the locations of maxima in the image and their presumed locations in real space. This fit precisely corrects for any nonlinear thermal drift or piezoelectric hysteresis in the (xy) image plane during data acquisition. The data in the equivalent unit cells of the images were averaged together to make a composite unit cell for each tunneling gap. The composite unit cell was Fourier filtered to remove spatial frequencies higher than those which could represent real data. The resulting average unit cells (repeated three times in each direction) are shown in Fig. 8.

Measurements are made of the relative tip height at the four high-symmetry points in these unit cells. Unlike the theoretical results, the absolute height of the STM tip over the surface cannot be determined experimentally; only the relative tip height within the set of data is measurable. These numerical image data, in the same form as the theoretical data in Fig. 5, are shown in Fig. 9. Due to the symmetry of the surface, some of the high-symmetry points (B and Mo) are present more than once in each overlayer surface cell. These locations have more than one data point associated with them.

A completely symmetric tip termination should produce images in which all equivalent points are equal. However, in all of the data sets, including that shown in Fig. 9, some asymmetry was observed. In the data of Fig. 9 this asymmetry is most severe in the middle range of gap resistance at the Mo location, and disappears at high and low gaps. Changes in the asymmetry with gap resistance qualitatively shows the changes in image contrast with gap resistance predicted by the theory, albeit for a nonideal tip. In this case, the tip might have been a tilted dimer. At certain gap distances, the dimer atom which was further from the surface contributed more significantly to the current than at other gaps, perhaps as a result of interferences between the tunneling paths through the two atoms making up the dimer.

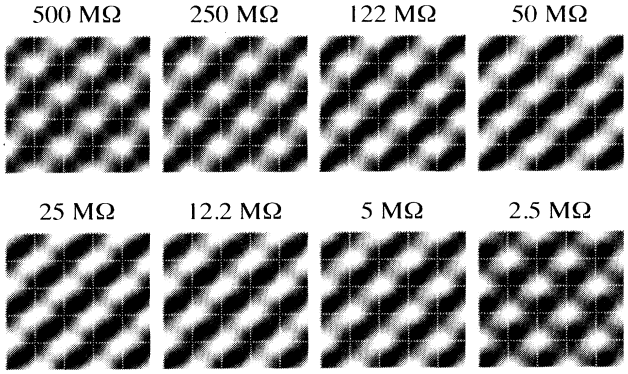

FIG. 8. Average unit cells over a range of gap resistance values. Each image is a 3×3 unit-cell plot of the composite unit cells derived by averaging approximately 20 unit cells from an image. All image data were acquired simultaneously with the multiple-gap imaging technique. The grid in the plots has vertices over the fourfold hollow sites of the Mo(100) lattice. While the maximum in the unit cells remain at the same place in all of the images, the contrast surrounding these maxima change with the gap resistance. In particular, these data show an asymmetry, due to an asymmetric tip, which appears most prominently in middle range of tunneling gaps and nearly disappears at high or low tunneling gaps.

Unfortunately, all of the acquired data showed some degree of asymmetry at least at some range of gap resistance. This indicates that the tip structure was in general less ideal than the models used in the theory, as might be expected. Various experimental methods were explored to produce completely symmetric tips, with only partial success. The least asymmetric images were selected for comparison to the theory.

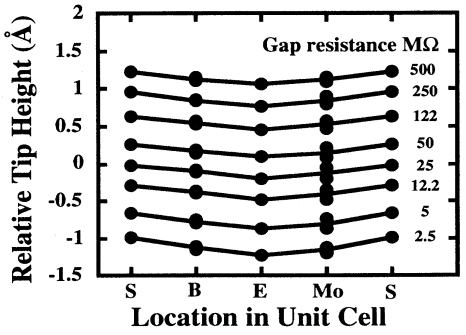

FIG. 9. Example of an experimental data set prepared for comparison to the theory. The data in this graph are extracted from the image data in Fig. 8. The data are in the same form as the theoretical data in Fig. 3, and can easily be compared quantitatively with it. An asymmetry appears at the Mo point in the unit cell in the middle range of tunneling gap resistance images. Two symmetrically equivalent data points have slightly different values.

VIII. STRUCTURE FIT

Each set of data from the experiment and the results of each trial structure calculations in the theory consists of the tip height at four high-symmetry positions in the overlayer unit cell, for a set of eight tunneling gap resistance values. The experimental and theoretical data were compared in the simplest possible way. The average rms difference in tip height between the experiment and theory was calculated for each trial structure and each set of experimental set. Experimental data for symmetrically equivalent points on the surface was averaged together (i.e., four B sites and two Mo sites). Since the absolute tip height was unknown in the experiment, the average experimental tip height was normalized to the average height in the theory for the entire data set. The complete formula used is

$$\mathbf{R}_{\mathrm{STM}}=\sqrt{\langle(z_{R,\mathbf{X}}-\zeta_{R,\mathbf{X}}-\langle z_{R,\mathbf{X}}-\zeta_{R,\mathbf{X}}\rangle)^2\rangle}\,, \tag{1}$$

where $Z_{R,\mathbf{X}}$ are the experimental data points and $\zeta_{R,\mathbf{X}}$ are the theoretical values at location $\mathbf{X}$ within the unit cell and gap resistance R. The quantities inside $\langle\ \rangle$ are averaged over the entire set of 32 data points. The quantity

$$\langle z_{R,\mathbf{X}}-\zeta_{R,\mathbf{X}}\rangle \tag{2}$$

is simply the average difference in tip height, which is subtracted from each difference to normalize the absolute tip height. Theoretical data points were interpolated over a continuous range of surface structures from the 25 individual calculations for each of the three tip types.

A representative set of results of the fit between the experimental data and the calculated images for each of the three model tips is shown in Fig. 10. These models show the R_{STM} factor as a function of the two structure parameters. The y axis represents the S height above the surface, while the x axis represents the Mo second-layer buckling. The fit for the Pt-atom-terminated model tip was always found to be much better than for the C, S, and Mo results. This is due to a better match of both the image shape and the rate of decay of tunneling current with tip-surface separation. The Pt fit plot shows a roughly triangular central region with a nearly constant R_{STM} factor. The R_{STM} factor rises quickly outside of this region.

Thus the fit results indicate that the termination of the tunneling tip in our experiments was always Pt. This is consistent with an uncontaminated predominantly Pt bulk tip. In addition, the results of the fit exclude a range of the possible surface structures. The best fit was for a S adsorbate height of 0.94 Å and a buckling of +0.10 Å. However, a range of about 20% of the selected parameter space produces nearly as good a fit.

The best-fit results of the surface structure differ from the dynamic LEED (Ref. 32) (S adsorbate height of 1.03

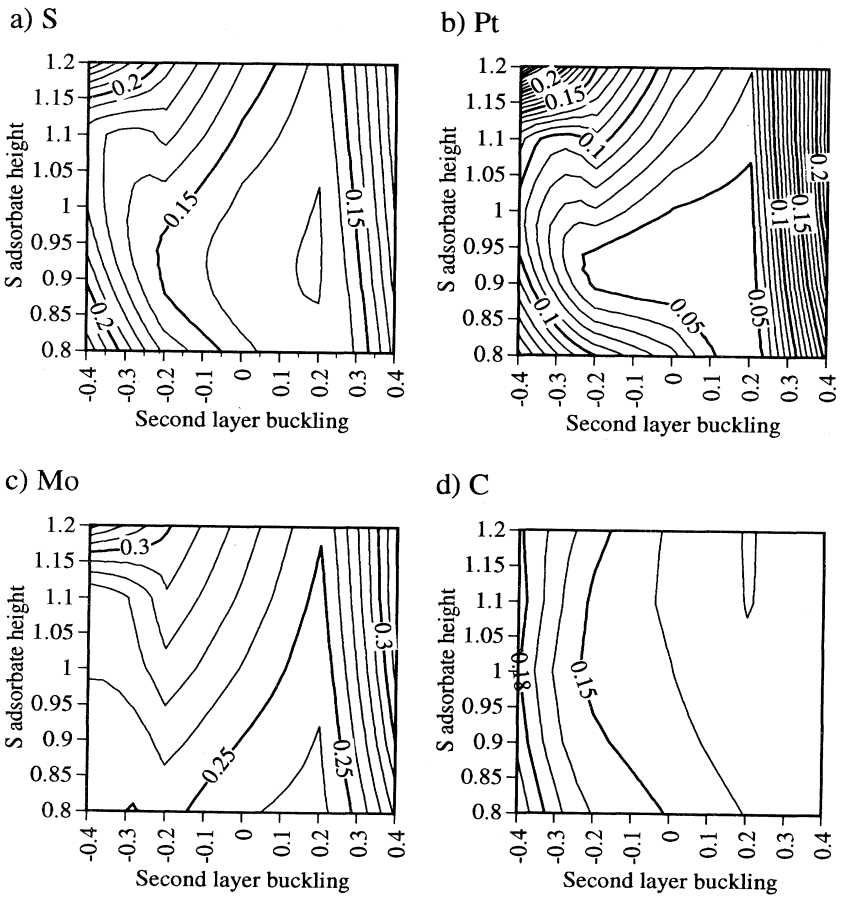

FIG. 10. The results of the fit of the experimental data to theory. All units in the plots are Å. These four contour plots show the variation of the fit quality factor, R_{STM}, with surface and tip structures. Each plot is for a different tip termination atom: S, Pt, C, or Mo. The x axis on each plot represents the buckling of the second Mo layer; the y axis represents the adsorption height of the S atom over the first Mo layer. The contours show the STM quality of fit factor R_{STM} defined in the text. The best fit is found for the Pt tip termination and a small range (about 20%) of the trial range of surface structures.

Å, buckling of −0.05 Å) results by approximately 0.1 Å. This error is significantly greater than the error expected for the LEED results. The most probable causes of the error in the STM results are an inadequate modeling of the tip, which the data indicate was always somewhat asymmetric. Additionally, the extended Hückel approximation of the electronic structure of the surface and tip produces inaccuracies in the theory. Finally, experimental error, such as small inaccuracies in the calibration of the piezoelectric elements moving the tip, could have produced some additional error.

IX. CONCLUSION

We have demonstrated that the contrast in STM images as a function of the tunneling gap is sensitive to the structure of the surface, and this fact may be utilized to determine quantitative information on the structure of the surface. By obtaining images over a wide range of tunneling gaps, the structure of the tip termination can be determined while simultaneously reducing the range of potential surface structures. As with LEED structure calculations, several different minima may be obtained in the fit between experimental and theory data. The data contained in the set of multiple gap images are smaller than that of most data sets used for dynamical LEED. However, STM is sensitive to the structure of fewer layers (only one or two) of the surface and thus fewer free structure parameters need to be fit. Additionally, a qualitative analysis of STM images often can provide a starting point for the structural determination by indicating the correct atomic binding site through symmetry arguments. In the future the STM data set may be expanded to include spectroscopic information as well as images acquired with several tip terminations. Further work is required to find out the number of free parameters which can be determined with STM image analysis. However, we expect that simultaneously ascertaining more than two or three parameters, as is common in dynamical LEED, will be difficult or impossible.

While STM is never likely to be as sensitive a probe of surface structure as diffraction techniques such as LEED, it can provide information inaccessible to these techniques. While here our technique was applied to a periodic surface to make comparison with LEED results possible, there is no reason why the same techniques cannot be applied to the study of defects on surfaces. In fact, the method may even be more accurate in this case, as images of the periodic areas of the surface may serve as a reference point with which to optimize the model of the tip structure.

There are several areas in which future work may improve the accuracy of the technique. The current definition of R_{STM} may overemphasize the rate of decay of the current with gap distance relative to the shape and corrugation of the images. This definition may be modified to reflect the important features in the image better from a structural point of view. The weakest point in the theory is the calculation of the Hamiltonian matrix elements with extended Hückel theory. In the future this calculation will be replaced with a more accurate method, derived from *ab initio* calculations of the surface electronic structure. In the experiment the greatest gains can be made through better control and characterization of the tip termination structure. It is likely that few methods will provide more accurate information on the tip termination than the analysis of the contrast of STM images produced with the tip. Therefore, the tip termination will be characterized by imaging a known surface structure before or simultaneously with the imaging of an unknown structure. Tips with more symmetric tip termination structures may be produced by etching single-crystal wire.

While a number of challenges remain ahead, we believe that the combination of multiple-gap imaging with theoretical calculations will allow the structure of simple chemisorbed systems on metal and defects in these overlayers to be determined from STM images.

*Author to whom all correspondence should be addressed. Electronic address: salmeron@stm.lbl.gov

[1]M. A. VanHove and S. Y. Tong, *Surface Crystallography by LEED: Theory, Computation, and Structural Results* (Springer-Verlag, Berlin, 1979).

[2]H. Niehus, W. Heiland, and E. Taglauer, Surf. Sci. Rep. **17**, 213 (1993).

[3]C. S. Fadley, in *Synchrotron Radiation Research: Advances in Surface and Interface Science,* edited by R. Z. Bachrach (Plenum, New York, 1992).

[4]J. E. Rowe, in *Synchrotron Radiation Research: Advances in Surface and Interface Science* (Ref. 3).

[5]J. C. Dunphy, P. Sautet, D. F. Ogletree, and M. B. Salmeron, J. Vac. Sci. Technol. A **11**, 1975 (1993).

[6]M. Tsukada, K. Kobayashi, and N. Isshiki, Surf. Sci. **242**, 12 (1991).

[7]B. J. McIntyre, P. Sautet, J. C. Dunphy, M. Salmeron, and G. A. Somorjai, J. Vac. Sci. Technol. B **12**, 1751 (1994).

[8]S. Rousset, S. Gauthier, O. Siboulet, S. W. Sacks, M. Belin, and J. Klein, Phys. Rev. Lett. **63**, 1265 (1989).

[9]L. Ruan, F. Besenbacher, I. Stensgaard, and E. Laegsaard, Phys. Rev. Lett. **70**, 4079 (1993).

[10]M. Tsukada, K. Kobayashi, N. Isshiki, and H. Kageshima, Surf. Sci. Rep. **13**, 265 (1991).

[11]A. A. Lucas, H. Morawitz, G. R. Henry, J.-P. Vigneron, P. Lambin, P. H. Cutler, and T. E. Feuchtwang, Phys. Rev. B **37**, 10 708 (1988).

[12]N. Garcia, C. Ocal, and F. Flores, Phys. Rev. Lett. **50**, 2002 (1983).

[13]H. Q. Nguyen, P. H. Cutler, T. E. Feuchtwang, T. Miskovski, and A. A. Lucas, Surf. Sci. **160**, 331 (1985).

[14]B. Das and J. Mahanty, Phys. Rev. B **36**, 898 (1987).

[15]G. Doyen, D. Drakova, and M. Scheffler, Phys. Rev. B **47**, 9778 (1993).

[16]J. Tersoff and D. R. Hamann, Phys. Rev. Lett. **50**, 1998 (1983).

[17]N. D. Lang, Phys. Rev. Lett. **56**, 1164 (1986).

[18]N. D. Lang, Phys. Rev. Lett. **58**, 45 (1987).
[19]P. Sautet and C. Joachim, Chem. Phys. Lett. **185**, 23 (1991).
[20]P. Sautet and C. Joachim, Ultramicroscopy **42-44**, 115 (1992).
[21]J. Bardeen, Phys. Rev. Lett. **6**, 57 (1961).
[22]R. M. Feenstra, J. A. Stroscio, J. Tersoff, and A. P. Fein, Phys. Rev. Lett. **58**, 1192 (1987).
[23]P. Sautet, J. Dunphy, D. F. Ogletree, and M. Salmeron, Surf. Sci. **295**, 347 (1993).
[24]P. Sautet, J. C. Dunphy, D. F. Ogletree, C. Joachim, and M. Salmeron, Surf. Sci. **315**, 127 (1994).
[25]A. Barbieri, D. Jentz, N. Materer, G. Held, J. Dunphy, D. F. Ogletree, P. Sautet, M. Salmeron, M. A. Vanhove, and G. A. Somorjai, Surf. Sci. **312**, 10 (1994).
[26]J. M. MacLauren, J. B. Pendry, P. J. Rous, D. K. Saldin, G. A. Somorjai, M. A. V. Hove, and D. D. Vvedensky, *A Handbook of Surface Structures* (Reidel, Holland, 1987).
[27]P. Sautet and M. L. Bocquet, Surf. Sci. **304**, L445 (1994).
[28]M. L. Bocquet and P. Sautet (unpublished).
[29]R. Landauer, Philos. Mag. **21**, 863 (1970).
[30]E. Clementi and C. Roetti, At. Data Nucl. Data Tables **14**, 177 (1974).
[31]J. H. Ammeter, H. B. Bürgi, J. C. Thibeault, and R. Hoffmann, Chem. Soc. **100**, 3686 (1978).
[32]D. Jentz, S. Rizzi, A. Barbieri, D. Kelly, M. A. VanHove, and G. A. Somorjai Surf. Sci. **329**, 14 (1995).
[33]D. M. Zeglinski, D. F. Ogletree, J. T. P. Beebe, R. Q. Hwang, G. A. Somorjai, and M. Salmeron, Rev. Sci. Instrum. **61**, 3769 (1990).
[34]J. C. Dunphy, C. Knight, P. Sautet, D. F. Ogletree, M. Salmeron, and G. A. Somorjai, Surf. Sci. **280**, 313 (1993).
[35]S. Rousset, S. Gauthier, O. Siboulet, W. Sachs, M. Belin, and J. Klein, J. Vac. Sci. Technol. A **8**, 302 (1990).
[36]V. Maurice and P. Marcus, Surf. Sci. **262**, L59 (1992).
[37]A. J. Gellman, J. C. Dunphy, and M. Salmeron, Langmuir **8**, 534 (1992).
[38]D. M. Eigler and E. K. Schweizer, Nature **344**, 524 (1990).
[39]M. Salmeron, D. F. Ogletree, C. Ocal, H.-C. Wang, G. Neubauer, W. Kolbe, and G. Meyers, J. Vac. Sci. Technol. B **9**, 1347 (1991).

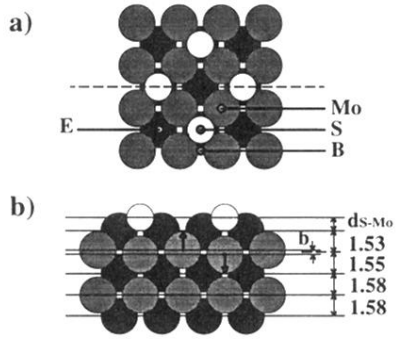

FIG. 1. A model of the $c(2\times2)$S-Mo(100) surface. (a) Top view. Every other fourfold hollow site contains a S adsorbate atom, shown in white. There are four high-symmetry sites on the surface: the location of the adsorbed sulfur atom (S), the bridge site (B), the empty hollow site (E), and over a Mo substrate atom (Mo). (b) Cross section. There are several numerical parameters which describe the surface structure. Two of these are determined by the analysis of the STM image data: the height of the sulfur atom over the surface ($d_{\text{S-Mo}}$) and the second-layer Mo buckling (b). Here the buckling (b) sign is defined as positive when the Mo atom under the sulfur adsorbate moves up toward it. (A negative buckling is indicated in the figure.) The other parameters, which specify the interlayer spacing of the Mo, are set to the values determined by a dynamical LEED study. These values are very close to the bulk layer spacing.

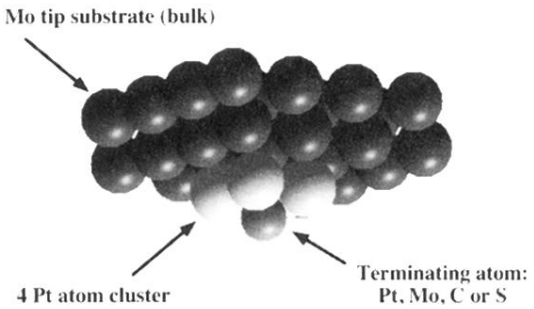

FIG. 2. Model tips used in the theory. The tip model contains three parts: the bulk, a cluster, and a termination atom. Throughout the tip all nearest-neighbor atomic separations are set to the sum of the covalent radii of the two neighbors. The bulk tip consists of Mo (the sample material) for simplicity. A four-atom Pt cluster is attached to the bulk to model the Pt alloy tip used in the experiment. A single atom is attached to this cluster. This tip termination atom is chosen from a set of likely experimental tip termination structures: Pt for a clean tip and S, C, or Mo for a contaminated tip.

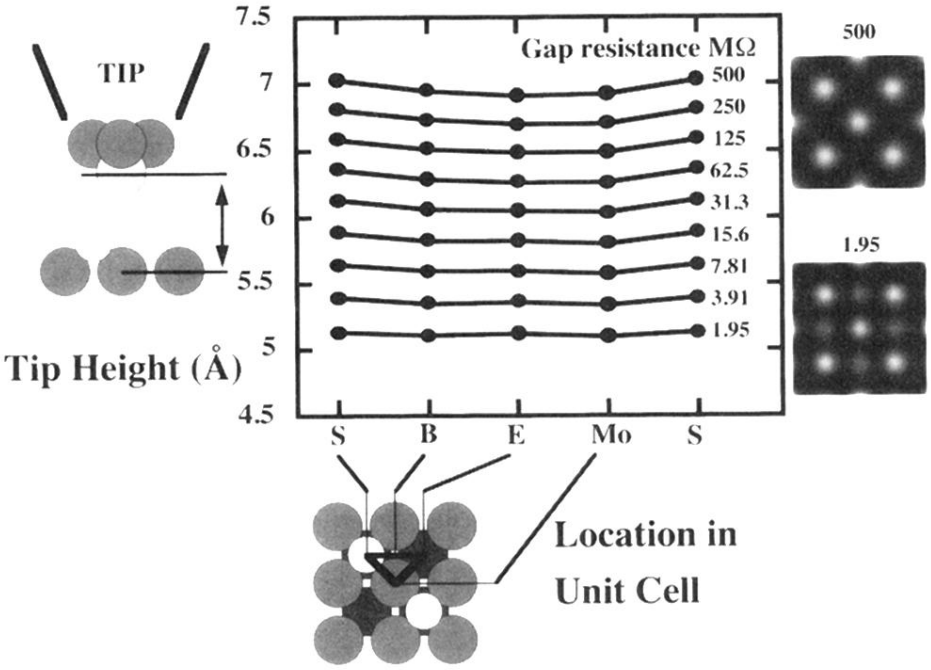

FIG. 3. Theoretical image shape plot for a single surface and tip structure. Each curve in this graph represents the distance from the tip to the surface at a specific tunneling gap resistance at the four high-symmetry sites on the surface, shown in the model below the graph. The distance between the tip and surface is defined as the distance between the center of the atom terminating the tip and the center of the first layer of Mo atoms on the surface. The tunneling gaps range from 2 to 500 MΩ by factors of 2. To the right of the plot are simulated images corresponding to the highest and lowest values of the tunneling gap. The contrast and corrugation of STM images varies markedly as a function of tunneling gap resistance.

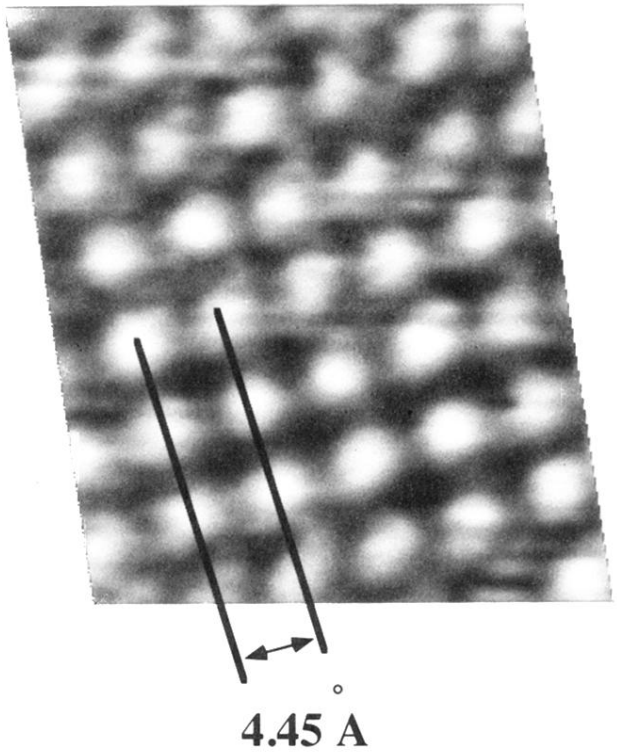

FIG. 5. A topographic STM image of $c(2\times2)$-ordered S on Mo(100). The maxima in the image are separated by 4.45 Å or $\sqrt{2}$Mo(100) lattice constants. This distance corresponds to the separation of the sulfur adsorbates. Therefore, each maximum is associated with one S and two Mo surface atoms. Defect sites in the lattice always appear as a missing maximum, indicating that the maxima correspond to the location of adsorbed S atoms.

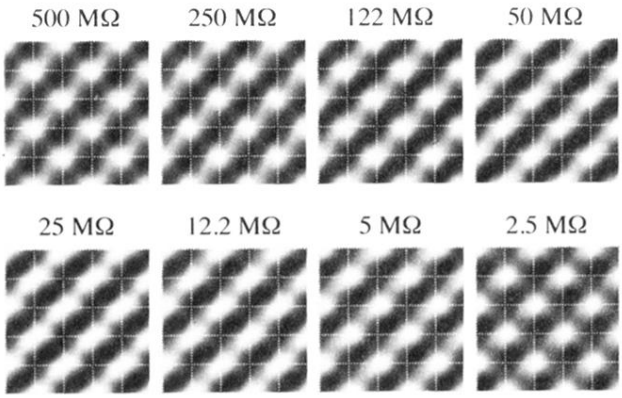

FIG. 8. Average unit cells over a range of gap resistance values. Each image is a 3×3 unit-cell plot of the composite unit cells derived by averaging approximately 20 unit cells from an image. All image data were acquired simultaneously with the multiple-gap imaging technique. The grid in the plots has vertices over the fourfold hollow sites of the Mo(100) lattice. While the maximum in the unit cells remain at the same place in all of the images, the contrast surrounding these maxima change with the gap resistance. In particular, these data show an asymmetry, due to an asymmetric tip, which appears most prominently in middle range of tunneling gaps and nearly disappears at high or low tunneling gaps.